Chiral Orbital-Angular Momentum in the Surface States of Bi_2Se_3

Seung Ryong Park,[1,*] Jinhee Han,[1] Chul Kim,[1] Yoon Young Koh,[1] Changyoung Kim,[1,†] Hyungjun Lee,[1] Hyoung Joon Choi,[1,‡] Jung Hoon Han,[2] Kyung Dong Lee,[3] Nam Jung Hur,[3] Masashi Arita,[4] Kenya Shimada,[4] Hirofumi Namatame,[4] and Masaki Taniguchi[4]

[1]*Institute of Physics and Applied Physics, Yonsei University, Seoul 120-749, Korea*
[2]*Department of Physics and BK21 Physics Research Division, Sungkyunkwan University, Suwon 440-746, Korea*
[3]*Department of Physics, Inha University, Incheon 402-751, Korea*
[4]*Hiroshima Synchrotron Radiation Center, Hiroshima University, Higashi-Hiroshima, Hiroshima 739-0046, Japan*
(Received 7 October 2011; published 25 January 2012)

We performed angle-resolved photoemission (ARPES) experiments with circularly polarized light and first-principles density functional calculation with spin-orbit coupling to study surface states of a topological insulator Bi_2Se_3. We observed circular dichroism (CD) as large as 30% in the ARPES data with upper and lower Dirac cones showing opposite signs in CD. The observed CD is attributed to the existence of local orbital-angular momentum (OAM). First-principles calculation shows that OAM in the surface states is significant and is locked to the electron momentum in the opposite direction to the spin, forming chiral OAM states. Our finding opens a new possibility for strong light-induced spin-polarized current in surface states. We also provide a proof for local OAM origin of the CD in ARPES.

DOI: 10.1103/PhysRevLett.108.046805 PACS numbers: 73.20.At, 71.15.Mb, 71.70.Ej, 74.25.Jb

Topological insulators (TIs) are a new class of materials that distinguish themselves from ordinary insulators by their topological properties [1,2]. Among the various properties of TIs, probably the most exciting one is the fact that they always have metallic surface states [3–8]. These surface states are topologically protected from perturbation by the time reversal symmetry. Moreover, electron spin of the surface state is locked into the momentum, making a chiral spin structure [7]. This spin texture suppresses backscattering [9–11] and thus promotes the possibility for TIs to be used for spin conserving media in spintronics [12]. Locking of the electron spin to the momentum comes from a combination of strong spin-orbit interaction and inversion symmetry breaking at the surface. The latter effect, known as the Rashba effect, occurs on the surfaces of many materials and produces spin degeneracy-lifted surface states [13], such as Au(111) surface states [14].

While chiral spin texture is well studied, orbital-angular momentum (OAM) is in many cases assumed to be quenched. Indeed, in recent studies of TIs, surface states are found to have approximately p_z character for which the OAM is quenched due to crystal field splitting [4]. Even though this may be a reasonable assumption for ordinary materials, there must be some tendency to restore a local OAM in high-Z materials with strong spin-orbit interaction, and the local OAM must also have chiral structure by symmetry [15]. The existence of chiral OAM in the surface states is important because it can provide electrostatic energy through electric dipole and surface electric field interaction [16]. This is a crucial feature in the *quantitative* description of Dirac conelike surface state dispersions. Chiral OAM is also important in optical properties of TI, since the orbital part of the total wave function directly couples to the electric field of light.

In order to investigate OAM in the surface states of TIs, we measured circular dichroism (CD) in angle-resolved photoemission spectroscopy (ARPES) from Bi_2Se_3, one of the widest band gap topological insulators [4,5]. We also performed first-principles calculation. In this Letter, we report strong CD in ARPES from the surface states of Bi_2Se_3, indicating that the surface states possess substantial chiral OAM. First-principles calculation also reveals chiral OAM with a sizable magnitude, proving the conclusion extracted from the experimental results. We discuss light-induced strong spin (and also OAM) polarized current from the surface states, which is directly deduced from the existence of substantial chiral OAM.

Single crystals of Bi_2Se_3 were grown by a self-flux method, following the previously reported technique [17]. ARPES measurements were performed at the beam line 9A of HiSOR equipped with a VG-SCIENTA R4000 analyzer. Data were taken with left- (LCP) and right-circularly polarized (RCP) 10 and 13 eV photons. The total energy resolution was set to be 10 meV, and the angular resolution was 0.1°. Samples were cleaved *in situ* and the chamber pressure was about 5×10^{-11} Torr. The measurement temperature was kept at 15 K. First-principles density functional calculations for the electronic structure of Bi_2Se_3 are based on *ab initio* norm-conserving pseudopotentials [18] and the Perdew-Burke-Ernzerhof-type generalized gradient approximation [19], as implemented in the SIESTA package [20]. We included the spin-orbit coupling in SIESTA. A supercell is used to obtain the electronic structure of a slab of Bi_2Se_3, which consists of 10 quintuple layers [21].

Depicted in Fig. 1(a) is the experimental geometry. The Bi_2Se_3 surface is in the xy plane. Circularly polarized lights come in at 40° to the xy plane in the xz plane. Photoemission intensity from the surface states is recorded as functions of energy and momentum for RCP and LCP light. In Figs. 1(b) and 1(c), we plot in the momentum space the ARPES intensity at the Fermi level taken with $h\nu = 13$ eV. The Fermi surface (FS) is where the ARPES intensity is high and has a hexagonal shape, consistent with published data [22]. The skewness in the FS shape is an experimental artifact but does not affect our discussion. As for the intensity, we note that it is not uniform along the FS, which means that the photoemission matrix element has momentum dependence. Comparing the two data sets, we see a very clear difference between the two FSs taken with two different circular polarizations. We see higher intensity on the negative k_y side for RCP but on the positive k_y side for LCP lights. To see CD more clearly, we subtract LCP data from RCP data and plot the difference data in Fig. 1(d). The intensity profile of the FS is antisymmetric about the horizontal axis ($k_y = 0$); the $+k_y$ side is negative while the $-k_y$ side is positive. For a quantitative analysis, we define CD by the difference in the ARPES intensities taken with two polarizations normalized by the sum of the two; that is, CD = (RCP − LCP)/(RCP + LCP). We plot in Fig. 1(e) CD at the Fermi level as a function of azimuthal angle Ω. Also plotted in the figure is the best sine curve fit to the experimental data. One can see that CD is as large as about 30% at $\Omega = \pi/2$ and $3\pi/2$. We note that experimental data deviate from the sine curve. Such deviation originates mainly from the out-of-plane component of the spin polarization [23,24]. This issue is out of the scope of this Letter and thus is not discussed. This issue has been discussed in a recent report [25].

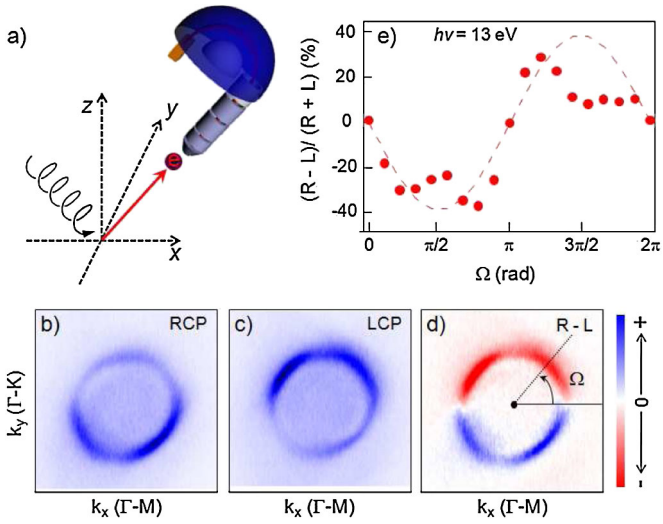

FIG. 1 (color online). (a) Experimental geometry used in the study. Bi_2Se_3 surface is in the xy plane. Circularly polarized photons represented by the helical arrows travel in the xz plane and the photon incidence angle is 40° to the sample surface. Fermi surface maps with 13 eV (b) RCP and (c) LCP light as well as (d) their difference (RCP − LCP) are plotted. Azimuthal angle Ω is defined as the angle from the positive k_x axis. (e) CD in ARPES at the Fermi level along the Fermi surface as a function of Ω. Difference between RCP and LCP is normalized by the sum of them. The dashed curve is the best sine function fit of the experimental data.

It is informative to see the binding energy dependent behavior of the CD from the surface states. We found that low energy photons have to be used to separate out the surface state information by suppressing the bulk intensity [8]. We used 10 eV photons to take CD data. Similar to Fig. 1(d), we plot in Fig. 2(a) the difference data (RCP-LCP) at the Fermi energy. Even though it has fewer number of momentum steps along the k_y direction compared to the 13 eV data, the dichroic behavior at the Fermi energy is roughly similar. The dichroic behavior is the most prominent along the k_y axis [dashed line in Fig. 2(a)]. We plot the E vs k data along the dashed line in Fig. 2(b). Dirac conelike bands of the surface states with the Dirac point at 0.3 eV are seen as expected. On the other hand, the intensity behavior of the two bands is opposite: the negative slope side has positive value while the positive side has negative value. Other than the Dirac conelike bands, states between 0.5 and 0.7 eV in the main valence band show CD,

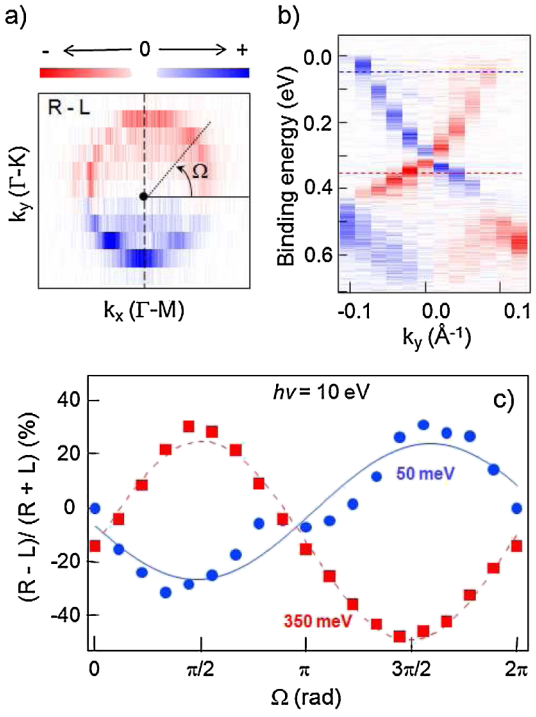

FIG. 2 (color online). (a) RCP − LCP data taken with 10 eV photons. (b) E vs k ARPES data along the dashed line in (a) ($k_x = 0$ cut). (c) CD in ARPES as a function of Ω at 50 (blue circle) and 350 (red square) meV binding energy. The energy positions are marked by the dashed lines in (b). Difference between RCP and LCP is normalized by the sum of them and the lines are the best sine function fits of the experimental data.

but no sign of CD was observed for the states beyond 0.7 eV. We plot in Fig. 2(c) CD at 50 and 350 meV binding energies as a function of azimuthal angle Ω defined in Fig. 2(a). CDs for the binding energies above and below the Dirac point oscillate with a periodicity of 2π but are out of phase by π. Also plotted in the figure are the best sine curve fits to the experimental data. One can see that CD is as large as 30% at $\Omega = \pi/2$ and $3\pi/2$.

What is causing the observed CD? In some cases, CD in ARPES can result from chiral experimental geometry effect [26,27]. However, a phase shift of π between the data below and above the Dirac point as well as an almost constant dichotic signal regardless of the distance from the Γ point shown in Fig. 2 cannot be explained by a simple chiral experimental geometry effect [26,27]. In addition, CD in ARPES as large as 30% is not expected in that case.

We argue that the observed CD is due to the existence of large chiral OAM in the surface states. The incident light at 40° is a linear sum of light propagating in the xy and yz planes (where z is the surface normal). First, let us focus on the component in the xy plane propagating along the x axis. Such a light can deliver $+1$ (RCP) or -1 (LCP) OAM to the magnetic quantum number (m_x) of the electronic state due to the dipole selection rule. Let us assume that the initial state at $\Omega = 3\pi/2$ has $m_x = 1$. This state will be projected to $m_x = 2$ and $m_x = 0$ states by RCP and LCP photons, respectively. The difference between transition matrix elements for $m_x = 2$ and $m_x = 0$ photoelectron final states should result in CD. The CD can be shown to be roughly proportional to $\hat{m} \cdot \hat{k}_{\mathrm{ph}}$, where $\hat{m}$ is the OAM direction and $\hat{k}_{\mathrm{ph}}$ is the incoming photon direction [15]. A detailed derivation of the relationship between CD and OAM can be found in the Supplemental Material [28]. We note a related work on graphene in which case CD comes from the existence of pseudospin [29]. The sinusoidal CD in Figs. 1(e) and 2(c) suggests that the OAM direction has a chiral structure and is perpendicular to the electron momentum as in the case of spins. In addition, one can find from Fig. 2(c) that the upper and lower Dirac cones have opposite OAM chirality.

We take a further step to directly prove the existence of chiral OAM. We performed first-principles calculations within generalized gradient approximation on a Bi_2Se_3 slab. The overall band structure is consistent with the published result [4]. In Fig. 3(a), we plot the crystal structure of the first Bi_2Se_3 quintuple layer along with the real space electron density of the surface state as a function of the distance from the surface. Note that the electron density is not localized at the very surface atomic layer but is distributed over the first quintuple layer.

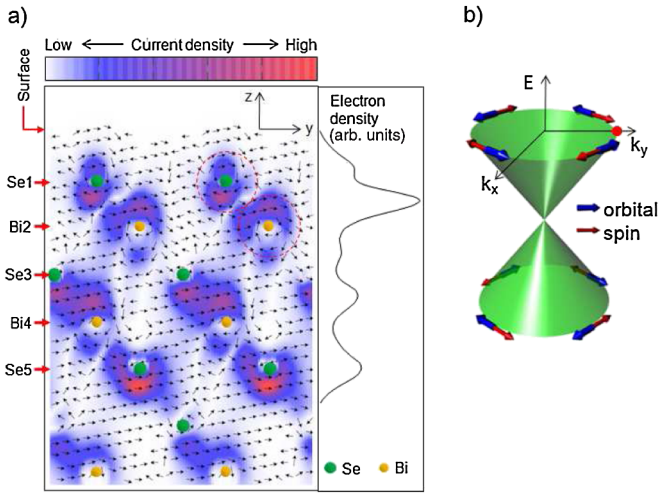

FIG. 3 (color online). (a) Crystal structure of Bi_2Se_3, showing the first quintuple layer. Direction and magnitude of the electron current density of a surface state are shown by arrows and in color scale, respectively. Shown on the right is the depth distribution of the surface state electron density. (b) Schematic band dispersion and OAM/spin configuration in the surface states.

We evaluate the local OAM of a surface state around each atom in the first quintuple layer by calculating the expectation values of the angular momentum operators using the projection of the surface state wave function onto three p orbitals of each atom (see the Supplemental Material [28] for details on the calculation method) [30]. Table I lists calculated values at each atomic site. Column 1 is the electron occupation of the three p orbitals obtained from the square of the projected wave function, which is the largest for Se_1 and the smallest for Se_3. Note that occupation numbers only sum up to 0.387 because they count the surface state wave function only in regions near the atoms in the first quintuple layer. Columns 2–4 list OAM expectation values calculated with the surface state at E_F and $\Omega = \pi/2$ [marked by the red dot in Fig. 3(b)] in

TABLE I. Listed are electron occupation, OAM, and normalized OAM values for the surface state at $\Omega = \pi/2$. Values are calculated by projecting the surface state on p orbitals of each atom. Angular momentum is given in units of $\hbar$.

	Occupation	$\langle L_x \rangle$	$\langle L_y \rangle$	$\langle L_z \rangle$	$\langle L_x \rangle_{\mathrm{norm}}$	$\langle L_y \rangle_{\mathrm{norm}}$	$\langle L_z \rangle_{\mathrm{norm}}$
Se_1	0.118	−0.034	0	0.010	−0.313	0	0.051
Bi_2	0.070	−0.051	0	0.001	−0.783	0	0.028
Se_3	0.023	0.016	0	0.002	0.703	0	0.088
Bi_4	0.088	−0.055	0	0.002	−0.581	0	0.011
Se_5	0.088	0.037	0	0.006	0.384	0	0.113

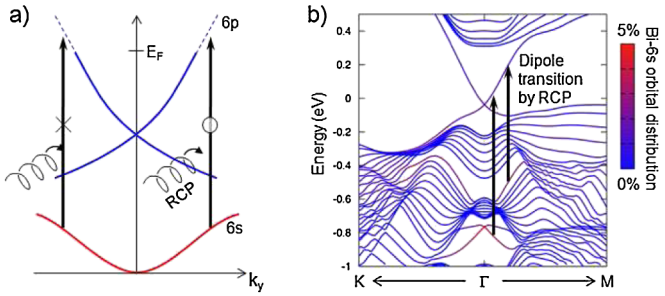

FIG. 4 (color online). (a) With RCP light, transition from 6s states to surface states is allowed on the positive momentum side where $m_x = 1$ while inhibited for the negative momentum side ($m_x = -1$), resulting in current with spin polarization in the x direction. (b) Distribution of the Bi_2 6s orbital in the band structure is shown in color scale. The band structure is from a 10 quintuple layer slab calculation.

units of $\hbar$. OAM is indeed nonzero, and is especially large for Bi atoms while values for Se atoms are small or even have the opposite sign. Since the major contribution comes from Bi atoms, we look at the values for Bi atoms. Note that orbital-angular momenta for Bi atoms are pointing in the negative x direction, which is opposite to the spin direction. The expectation values may also be normalized by the electron occupation listed in column 1. Normalized values may be a good measure of the OAM strength, with the maximum value of $\hbar$ for a p electron. They are listed in columns 5–7. Values for Bi atoms are large as expected, close to 80% of the full value of $\hbar$.

Even though the expectation values listed in Table I already confirm the existence of OAM, we can also visualize it. Plotted in Fig. 3(a) is the current density for the surface state at E_F and $\Omega = \pi/2$ [represented by the red dot in Fig. 3(b)]. The arrows represent the direction of the current while the density is shown in the color scale. Overall, the current is flowing to the positive y direction as expected. Looking at more details, one finds the current rotating locally around atoms and it does so in the direction that produces an OAM in the negative x direction (except Se_3 and Se_5 atoms). All these results prove that OAM of the surface states in Bi_2Se_3 form chiral states.

An important implication of the large OAM in the surface states is that very strong spin (and also OAM) polarized current in surface states can be induced by light. From the dipole section rule, an electron with s-orbital character can be excited to the surface states (p orbitals) by a photon. In addition, existence of OAM allows us to use circularly polarized photons to excite electrons only in a certain part of the Brillouin zone. As the surface states are spin polarized, selective excitation of electrons should result in spin-polarized current. Figure 4(a) schematically shows the process. RCP photons, for example, excite electrons with positive momentum, resulting in current in the positive direction with spins polarized along the x direction.

Then the question is whether we have states with s-orbital character. Figure 4(b) shows in a color scale the contribution from the 6s orbital of a Bi_2 atom to the near E_F states. Although Bi 6s states mostly reside in the valence band around 10 eV binding energy [31], a small portion of them exist near E_F, as shown in Fig. 4(b). In particular, bands at about 0.6 and 0.8 eV binding energies near the Γ point have about 3% and 5% of Bi 6s orbital components, respectively. We calculated the transition rates between the two states shown in Fig. 4(b) for 0.7 eV LCP and RCP light (equivalently, transition rates for k and $-k$ states with a polarization). The ratio between the two transition rates is found to be about 3.5, meaning that RCP light will induce 3.5 times more current in the k direction compared to the $-k$ direction. Therefore, very strong light-induced spin and OAM polarized current can be realized in the surface states of TIs. It was recently reported that charge transport dominantly occurs in the surface states for high quality TI thin films [32], which means that light-induced spin and OAM polarized current became more realistic. It could then be used for optospintronic applications [33].

Experimental work is supported by the KICOS through Grant No. K20602000008 and by Mid-career Researcher Program through NRF grant funded by the MEST (No. 2010-0018092). The computation part was supported by the NRF of Korea (Grant No. 2011-0018306) and computational resources have been provided by KISTI Supercomputing Center (Project No. KSC-2011-C2-04). ARPES measurements were performed with the approval of the Proposal Assessing Committee of HSRC (Proposal No. 09-A-49).

*Present address: Department of Physics, University of Colorado at Boulder, Boulder, Colorado 80309, USA.
†changyoung@yonsei.ac.kr
‡h.j.choi@yonsei.ac.kr

[1] L. Fu, C. L. Kane, and E. J. Mele, Phys. Rev. Lett. **98**, 106803 (2007).
[2] J. E. Moore and L. Balents, Phys. Rev. B **75**, 121306(R) (2007).
[3] D. Hsieh *et al.*, Nature (London) **452**, 970 (2008).
[4] H. Zhang *et al.*, Nature Phys. **5**, 438 (2009).
[5] Y. Xia *et al.*, Nature Phys. **5**, 398 (2009).
[6] Y. L. Chen *et al.*, Science **325**, 178 (2009).
[7] D. Hsieh *et al.*, Nature (London) **460**, 1101 (2009).
[8] S. R. Park *et al.*, Phys. Rev. B **81**, 041405(R) (2010).
[9] P. Roushan *et al.*, Nature (London) **460**, 1106 (2009).
[10] T. Zhang *et al.*, Phys. Rev. Lett. **103**, 266803 (2009).
[11] Z. Alpichshev *et al.*, Phys. Rev. Lett. **104**, 016401 (2010).
[12] D. X. Qu *et al.*, Science **329**, 821 (2010).
[13] Y. A. Bychkov and E. I. Rashba, JETP Lett. **39**, 78 (1984).
[14] F. Reinert, G. Nicolay, S. Schmidt, D. Ehm, and S. Hüfner, Phys. Rev. B **63**, 115415 (2001).
[15] J.-H. Park *et al.*, arXiv:1112.1821v1.

[16] S. R. Park, C. H. Kim, J. Yu, J. H. Han, and C. Kim, Phys. Rev. Lett. **107**, 156803 (2011).
[17] Y. S. Hor *et al.*, Phys. Rev. B **79**, 195208 (2009).
[18] N. Troullier and J. L. Martins, Phys. Rev. B **43**, 1993 (1991).
[19] J. P. Perdew, K. Burke, and M. Ernzerhof, Phys. Rev. Lett. **77**, 3865 (1996).
[20] D. Sánchez-Portal, P. Ordejón, E. Artacho, and J. M. Soler, Int. J. Quantum Chem. **65**, 453 (1997).
[21] W. Zhang *et al.*, New J. Phys. **12**, 065013 (2010).
[22] K. Kuroda *et al.*, Phys. Rev. Lett. **105**, 076802 (2010).
[23] L. Fu, Phys. Rev. Lett. **103**, 266801 (2009).
[24] S. Souma *et al.*, Phys. Rev. Lett. **106**, 216803 (2011).
[25] Y. H. Wang *et al.*, Phys. Rev. Lett. **107**, 207602 (2011).
[26] R. L. Dubs, S. N. Dixit, and V. McKoy, Phys. Rev. Lett. **54**, 1249 (1985).
[27] C. Westphal, J. Bansmann, M. Getzlaff, and G. Schonhense, Phys. Rev. Lett. **63**, 151 (1989).
[28] See Supplemental Material at http://link.aps.org/supplemental/10.1103/PhysRevLett.108.046805 for the calculation method for extracting OAM and for proof of local OAM origin of circular dichroism in ARPES.
[29] Y. Liu, G. Bian, T. Miller, and T.-C. Chiang, Phys. Rev. Lett. **107**, 166803 (2011).
[30] B. I. Min and Y.-R. Jang, J. Phys. Condens. Matter **3**, 5131 (1991).
[31] S. K. Mishra, S. Satpathy, and O. Jepsen, J. Phys. Condens. Matter **9**, 461 (1997).
[32] N. Bansal *et al.*, arXiv:1104.5709.
[33] I. Žutić, J. Fabian, and S. D. Sarma, Rev. Mod. Phys. **76**, 323 (2004).